Virus-host metabolic interactions: using metabolomics to probe oxidative stress, inflammation and systemic immunity

Schoeman, J.C.

Chapter 6

Metabolic characterisation of the natural progression of chronic hepatitis B

Johannes C. Schoeman, Jun Hou, Amy C. Harms, Rob J. Vreeken, Ruud Berger, Thomas Hankemeier, and Andre Boonstra

Genome Medicine (2016) - 10;8(1):64

Abstract

Worldwide, over 350 million people are chronically infected with the hepatitis B virus (HBV) and are at increased risk of developing progressive liver diseases. The confinement of HBV replication to the liver, which also acts as the central hub for metabolic and nutritional regulation emphasises the interlinked nature of host metabolism and the disease. Still, the metabolic processes operational during the distinct clinical phases of a chronic hepatitis B virus (HBV) infection - immune tolerant, immune active, inactive carrier, and HBeAg-negative hepatitis phases - remains unexplored. To investigate this, we conducted a targeted metabolomics approach on serum to determine the metabolic progression over the clinical phases of chronic HBV infection, using patient samples grouped based on their HBV-DNA, alanine aminotransferase and HBeAg serum levels. Our data illustrate the strength of metabolomics to provide insight into the metabolic dysregulation experienced during chronic HBV. The immune tolerant phase is characterised with the speculated viral hijacking of the glycerol-3-phosphate-NADH shuttle explaining the reduced glycerophospholipids and increased plasmalogen species, indicating a strong link to HBV replication. The persisting impairment of the choline glycerophospholipids, even during the inactive carrier phase with minimal HBV activity, alludes to possible metabolic imprinting effects. The progression of chronic HBV is associated with increased concentrations of very long chain triglycerides together with citrulline and ornithine, reflective of a dysregulated urea cycle peaking in the HBeAg-negative phase. The work presented here will aid in future studies to (i) validate and understand the implication of these metabolic changes using a thorough systems biology approach, (ii) monitor and predict disease severity as well as (iii) determine the therapeutic value of the glycerol-3-phosphate-NADH shuttle.

Background

Worldwide, over 350 million people are chronically infected with the hepatitis B virus (HBV) and are at increased risk of developing progressive liver diseases, including fibrosis, liver failure, or hepatocellular carcinoma (HCC) over the course of several decades [1,2]. Chronic HBV infection can be divided into four progressively distinct clinical phases based upon serum levels of HBV-DNA, alanine aminotransferase (ALT), and HBV e antigen (HBeAg). These four phases are: the immune tolerant (IT), immune active (IA), inactive carrier (IC), and HBeAg-negative (ENEG) phase. The increased ALT levels in the IA and ENEG phase reflect hepatic injury due to viral activity and immune activity. Even though these phases are used in clinical practise for deciding on therapeutic interventions [3], not much is known about the underlying metabolic mechanisms associated with each, and/or the progressive nature of the disease. HBV replicates in the liver, which also acts as the central hub for metabolic and nutritional regulation emphasising the interlinked nature of the metabolism and the disease. Hence, a clear metabolic understanding of the progressive driving forces and diverse clinical outcomes are important in the management of chronic hepatitis B, for instance to provide prediction markers for disease progression and candidate targets for therapeutic intervention. *In vitro* systems are not reliable models for chronic HBV since they do not represent the persistence, complexity and the progressive nature of the disease. Animal models do not appropriately mimic the pathogenic and immunological responses experienced during human HBV infection, hindering effective translational studies [4,5]. Thus, the use of material obtained from patients is crucial to study and understand chronic HBV.

Metabolomics is an established, continuously improving, tool used to study the metabolome through targeted or untargeted approaches, providing static observational and/or longitudinal readouts from a dynamic system [6–9]. Targeted metabolomics, which focuses on a predefined biology-driven subset of metabolite classes, is ideal for low concentration metabolites, whereas untargeted metabolomics is more suitable for measuring high concentration metabolites [10]. Metabolomics data aid in identifying and understanding the metabolic perturbations leading to dysregulated homeostasis and stress, e.g. during viral infection [11–14]. Subsequently, the contribution of these metabolic perturbations to the pathogenicity of the virus can be determined. Several metabolomics studies have been done to assess the metabolic host-pathogen interaction during a chronic HBV infection. Targeted metabolomics approaches have identified the phospholipids [15,16], triglycerides [15,17,18], sphingomyelins [15,19] and free fatty acid metabolism [16,20] as metabolic pathways affected during chronic HBV infection. Untargeted approaches have also been used to investigate metabolic changes experienced during chronic HBV [21–23], and have primarily focussed on HBV related cirrhosis and HCC [15,24–26].

Here we present the first discovery metabolomics study of chronic HBV, shedding light on the progressive metabolic alterations over the different clinical phases. We used targeted metabolomics platforms to illuminate the phospholipid, triglyceride, sphingomyelin, amino acid, acyl-carnitine, and signalling lipid profiles to characterise the progressive nature of chronic HBV infection. We identified the most profound changes in choline glycerophospholipids, plasmalogens, very long chain triglyceride species and urea cycle intermediates across the progression of the four clinical phases of chronic HBV. Our data supports the viral hijacking and persisting impairment of the glycerol-3-phosphate NADH shuttle, modulating the host lipid

profile. These events are central to understanding the metabolic perturbations reflective of the natural progression of chronic HBV.

Methods

Study population

Sixty-nine chronic HBV patients and nineteen healthy controls (HCs) were included in this discovery study. The blood was prospectively collected in SST tubes at the Erasmus MC. The blood was centrifuged to separate the serum and stored at -80°C until analysis. Patients were treatment naïve, and excluded in case of a co-infection with other chronic infections (HIV, HCV) or a body mass index of 31 or more. This study was conducted in accordance with the guidelines of the Declaration of Helsinki and the principles of Good Clinical Practice. The ethical review board of the Erasmus MC has approved the study, and informed consent was obtained from all patients who were asked to donate blood.

Definition of chronic HBV clinical phases

Serum ALT was measured on an automated analyzer, qualitative serum HBsAg, HBeAg, and anti-HBeAg antibodies were measured on an Architect Abbott analyzer, and serum HBV-DNA levels were measured using the COBAS AmpliPrep-COBAS Taq-Man HBVv2test (CAP-CTM; Roche Molecular Systems, Indianapolis, IN). Based on serum HBV DNA, ALT levels and HBeAg presence at the time of sampling, patients were categorized into four clinical HBV phases according to international guidelines [27]. IT patients (n=18) had detectable serum HBeAg and repetitive normal ALT values (<40 U/L). IA patients (n=12) and ENEG patients (n=19) had repetitive or intermittent abnormal serum ALT (>40 U/L) values, and HBV DNA levels >2,000 IU/mL. IC patients (n=20) patients were HBeAg-negative and had both repetitive normal ALT values (<40 IU/L) and HBV DNA levels below 20,000 IU/ mL.

Targeted LC-MS metabolomics

Targeted Metabolomics analyses were done using standard operating procedures from previously published methods. Detailed procedures and target lists are provided in the Supplemental methods with a brief overview of the five platforms used given in Table 6.1.

Quality control (QC) samples consisted of equally pooled volumes of all study samples. A set of QC samples were then included during the analyses of the experimental groups on the individual metabolomic platforms, and evenly distributed through the randomized samples prior to LC-MS analyses. In addition, independent duplicate samples (10-15%) were randomly selected where sample volume allowed.

Table 6.1: Metabolomics platforms. A brief overview of the platforms detailing volumes, sample preparation and analytical instruments.

Targeted Metabolomics Platform	Volume serum used (uL)	Sample Prep Method	Analytical platform	Metabolite class coverage	Platform Targets (n)		
					Total	Quality control passed	% Missing data
Biogenic amine [28]	5 µL	Protein precipitation & AccQTag derivatization	UPLC-TQMS	Amino acids, catecholamines & polyamines	100	38	0.03
Positive lipid [29]	10 µL	Isopropyl alcohol extraction	UPLC-QToF	Phospholipids, cholesterol esters, di/triglycerides & sphingomyelins	250	140	0.11
Negative lipid [29]	20 µL	Methanol extraction	UPLC-QToF	Free fatty acids & Phospholipids	150	59	0.17
Oxylipins [30]	250 µL	Oasis HLB SPE extraction	HPLC-MS/MS	Hydroxylated fatty acids, prostaglandins & thromboxanes	120	35	0.07
Acyl-carnitines	10 µL	Protein precipitation	UPLC- Xevo-TQMS	Acylcarnitines, TMAO, choline, Betaine	50	26	0

After LC-MS analyses, peak integration was done using the instrumental software, and the relative ratios between metabolites and their corresponding internal standards were determined. Using the QC samples and duplicate samples, a double-QC approach was applied to include metabolites that were reliably measured by the individual metabolomics platforms by reporting and using only those metabolites for which both duplicate samples and QC samples showed an RSD<30%. After QC, a data set comprising 88 cases and 314 metabolites were constructed, with all missing data being replaced by half the minimal intensity value of the corresponding metabolite.

Statistical data analyses

SPSS 21.0 (SPSS Inc., Chicago, IL, USA) was used for Fisher's exact tests on the patient cohort characteristics presented as frequencies, and ANOVA on the continuous values. A combination of univariate and multivariate bioinformatics approaches was performed using the R script–based online tool Metaboanalyst 3.0, a comprehensive tool suitable for analysing metabolomics data [31,32]. The metabolomics data sets were log transformed and auto-scaled prior to bioinformatics analyses. For the analyses between HCs and IT-patients, significant metabolites were identified per metabolomics platform based on the following criteria: *i*) a *p*-value < 0.05 using the independent student t-test, and ii. a fold change (FC) ≥ 1.20 or ≤ 0.80, indicating a 20% increase or decrease. The False discovery rate's q-values are reported for every reported *p*-value. The multivariate Principal component analyses (PCA) was also done to visual the natural distribution of the data.

The multivariate ANOVA test was used to identify the significant changes ($p < 0.05$) across the four clinical phases of chronic HBV in conjunction with K-means clustering. A K-means clustering was performed in MATLAB using *kmeans* and 'correlation' as the distance measure on the metabolites in order to examine changes in their levels during the course of chronic HBV, using all 314 metabolites and 88 patients. Its algorithm partitions the metabolites into K mutually exclusive clusters (k is the number of desired clusters), taking into account the measurement of each metabolites under multiple conditions, in this case HCs plus all 4 clinical phases. Within each cluster, metabolite measurement patterns are as close to each other as possible, while as far away from metabolites in other clusters as possible. The partition was repeated with metabolites reassigned

among clusters at each iteration until the sum of point-to-centroid distance reaches a minimum [33]. The pattern analysis was performed sequentially with k assigned with 12, 16, 20 and 24 each time.

Results

Baseline Characteristics of the study population.

For the metabolomics characterisation of chronic HBV infection, a cohort of treatment naïve patients was chosen, and patients with other comorbidities and/or advanced liver fibrosis were excluded from the study. Due to the progressive nature of chronic HBV infection over time, IT and IA patients are younger than IC and ENEG patients (p=0.03) (Table 6.2). The asymptomatic IT and IC groups have a larger female representation, due to routine HBsAg testing during pregnancy and subsequent referrals. This gender ratio is reversed in the IA and ENEG groups (Table 2). The ratios of HBV genotypes are evenly spread in the cohort, except for the IT and ENEG groups where genotypes B/C, and D are dominant, respectively (Table 6.2). Owing to the stringent definition criteria, differences in ALT (Fig. 6.1a) and HBV-DNA (Fig. 6.1b) levels are observed between the clinical phases.

Table 6.2. Baseline characteristics of the patient cohort.

Characteristics	Total cohort (N=88)	Healthy Control (HC) (N=19)	Immune tolerant (IT) (N=18)	HBeAg-positive active hepatitis (IA) (N=12)	Inactive carrier (IC) (N=20)	HBeAg-negative active hepatitis (ENEG) (N=19)
Demography						
Age, year (SE)	35.26 (11.58)	-	30.89 (1.77)	31.75 (2.60)	39.85 (3.02)	37.68 (2.75)
Gender, n (%) **						
Female	41	7 (17.1%)	13 (31.7%)	5 (12.2%)	14 (34.2%)	2 (4.9%)
Male	41	6 (14.6%)	5 (12.2%)	7 (17.1%)	6 (14.6%)	17 (41.5%)
		7 missing				
BMI, kg/m2 (SE)	24.64 (6.40)	-	25.93 (3.27)	23.08 (1.12)	24.41 (0.70)	24.66 (0.79)
Race, n (%) *						
Asian	44 (63.77%)	-	16 (36.4%)	9 (22.7%)	8 (18.21%)	10 (22.7%)
Caucasian	9 (13.04%)	-	0 (0.0%)	3 (33.3%)	2 (22.2%)	4 (44.4%)
African	8 (11.59%)	-	0 (0.0%)	0 (0.0%)	5 (62.5%)	3 (37.5%)
Other	8 (11.59%)	-	2 (25.0%)	0 (0.0%)	4 (50%)	2 (25.0%)
Virology						
log HBV DNA, IU/ml (SE) §	5.55 (2.82)	-	8.84 (0.07)	7.40 (0.57)	2.43 (0.15)	4.39 (0.30)
HBV Genotype A/B/C/D **	13/16/20/20	-	0/8/8/2	3/2/6/1	6/5/2/6	4/1/3/11
Chemistry/haematology						
ALT, IU/l (SE) §	48.17 (43.56)	-	24.50 (1.72)	88.83 (16.93)	23.90 (1.43)	69.53 (10.91)

BMI: Body mass index; SE: Standard Error

Fisher's exact *p*-value: * < 0.05; ** < 0.01; ANOVA *p*-value: § < 0.01

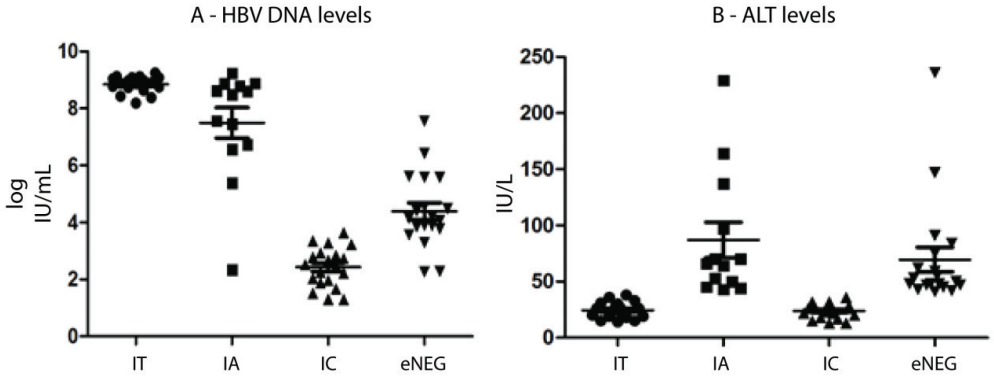

Figure 6.1: Clinical parameters. Baseline serum characteristics of chronic HBV patients divided into four clinical phases based on ALT and HBV DNA levels. Serum samples of 69 chronic HBV patients were measured for their levels of (a) HBV DNA and (b) ALT levels.

Metabolic characterisation of the IT phase of chronic HBV versus the healthy controls

To investigate and understand the metabolic alterations during the progressive clinical phases of a chronic HBV infection, we first characterised HC versus the IT phase, representing the onset of chronic HBV. Multivariate and univariate data analysis were performed to identify metabolic pathways altered in the IT phase. The PCA showed natural clustering with partial overlap observed between the HCs and IT sample groups (Figure S6.1). For univariate analysis, fold change in combination with t-tests were used, and the identified significant metabolites are visualised in a volcano plot (Fig. 6.2, (Table S6.1)). The volcano plot highlighted 92 significant metabolites belonging to the phospholipid, plasmalogen, triglyceride, amino acid, sphingomyelin, free fatty acid and acyl-carnitine metabolism listed in Table 6.3. Under closer inspection the univariate/supervised analysis reveals primarily uniform class responses indicating definite metabolic rearrangement. The down-regulated metabolites are dominated by triglycerides, phospholipids, lysophospholipids, and sphingomyelins metabolites in the IT phase compared to HCs. In contrast, plasmalogens (specialised vinyl ether-linked phospholipids), free fatty acids and acyl-carnitines classes presented with elevated levels in the IT phase compared to HCs. Clinically, the IT phase is characterised with high levels of HBV replication and negligible hepatic injury, hence the dysregulated lipid profile observed is most likely due to metabolic hijacking occurring during the HBV life cycle.

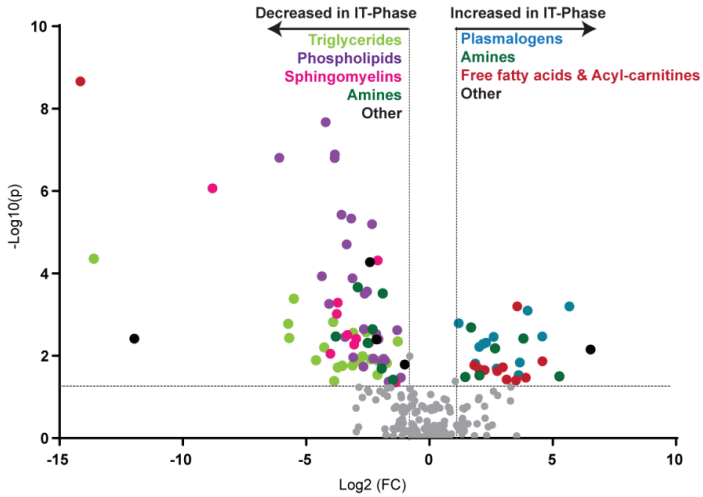

Figure 6.2: Volcano plot of the significant serum metabolites between the HCs and the IT phase. Metabolites with a fold change (X-axis) threshold of 2 and t-tests (Y-axis) threshold of 0.05 are identified as significant and represented by coloured circles ordered by the metabolite class. The further its position away from the (0,0) the more significant the metabolite. Metabolite classes are as followed: Triglycerides (green), Phospholipids (purple), Sphingomyelins (pink), Amines (orange), Plasmalogens (blue), Free fatty acids and acyl carnitines (Maroon) and others (Black).

Table 6.3: Significant serum metabolites identified between HCs and IT phase. The metabolites identified as significant based on t-test and fold change are divided into their different classes together with their trend. All metabolites had a *q*-value < 0.05 unless otherwise indicated.

Targeted Metabolomics Platform	Class	Metabolite species identified as significant between the HCs and IT phase	Trend in the IT-phase
		Phospholipids	
Positive Lipids	Phosphatidylcholines (PC)	C32:1; C32:2; C34:1; C34:3; C34:4; C36:3; C36:4; C36:6; C38:3;	Decreased
	Phosphatidylethanolamines (PE)	C38:4	Decreased
		Plasmalogens	
Positive Lipids	Plasmalogen phosphatidylcholines (pPC)	C34:2; C36:2; C36:3; C38:6;	Increased
	Plasmalogen phosphatidylethanolamines (PE)	C38:5; C38:7[#]	Increased
		Lysophospholipids	
Negative Lipids	Lysophosphatidylcholines (LPC)	*sn1*: C14:0; C15:0; C16:1; C18:1; C18:2; C18:3 (w3w6); C20:3 (w3w6); C20:3 (w9); C20:4; C22:4; C22:5 (w6) *sn2*: C14:0; C16:1; C18:1; C18:2; C18:3 (w3w6); C20:3 (w3w6); C20:4	Decreased
	Lysophosphatidylethanolamines (LPE)	C18:0; C18:1; C18:2[#]; C20:3 (w3w6); C20:4; C22:5[#] (w3)	Decreased
		Lysophospholipids	
Negative Lipids	Plasmalogen Lysophosphatidylcholines (pLPC)	C16:0; C16:1; C18:1; C18:2	Increased
		Triglycerides	
Positive Lipids	Triglycerides	C42:1; C44:2; C46:1; C46:2; C46:3; C48:1; C48:2; C48:3; C48:4[#]; C50:0; C50:1; C50:2; C50:3; C50:4; C50:5; C51:1; C51:2; C51:3; C52:1; C52:2; C54:1; C54:2; C55:2; C56:5; C58:5	Decreased
		Amines	
Amines	Amino acids	Tryptophan[#]	Decreased
	Glutathione	Glutathione	Decreased
	Dipeptides	γ-Glutamylglutamine	Decreased
	Amino acids metabolites	Kynurenine; Saccharopine	Decreased
	Hepatic injury	4-Hydroxyproline; Pipecolic acid	Increased
	Glycine metabolism	Betaine[#]; Sarcosine[#]	Increased
	Other	s-Methylcysteine	Increased
		Sphingomyelins	
Positive Lipids	Sphingomyelins (SM)	C18:1/14:0; C18:1/21:0; C18:1/23:0; C18:1/25:0; C18:1/25:1	Decreased
		Free fatty acids and Acyl-carnitines	
Negative Lipids	Free fatty acids (FFA)	C18:2; C20:2	Increased
Acyl-Carnitines	Acyl-Carnitines	Nonanoylcarnitine (C9:0Oleylcarnitine (C18:1)[#]; Linoleylcarnitine (C18:2)	Increased *Decreased
		Others	
Positive Lipids	Cholestrol Esters (CE)	C18:3	Decreased
Oxylipins	Oxylipins	5-HETrE*; 11-HDoHE[#]; 14-HDoHE[#]; 10-HDoHE[#]; 8,9-DiHETre[*,#]; 12,13-DiHOME[*,#]	Increased *Decreased

[#] *q*-value > 0.05

Metabolomics characterisation of the natural course of a chronic HBV infection

Given the interdependent nature of metabolic pathways, functionally related metabolites might present with similar responding patterns. To examine this, a K-means pattern analysis was performed on the total metabolomics data set comprising 88 cases and 314 metabolites. A pattern of 24 clusters was selected as the most distinct pattern describing the metabolomics data (Figure S6.2, Table S6.2). Subsequently, 6 of the 24

clusters were chosen to be studied further, based upon the profile and the number of metabolites (n>5) clustering within each, and the correlation between profiles and fluctuation of ALT and HBV DNA levels (Fig. 6.3). Pattern analysis identifies similar responding metabolites, but is not a measure of significance, and therefore an ANOVA approach was used between the four clinical phases to identify significantly changing metabolites (Table 6.4, Table S6.3).

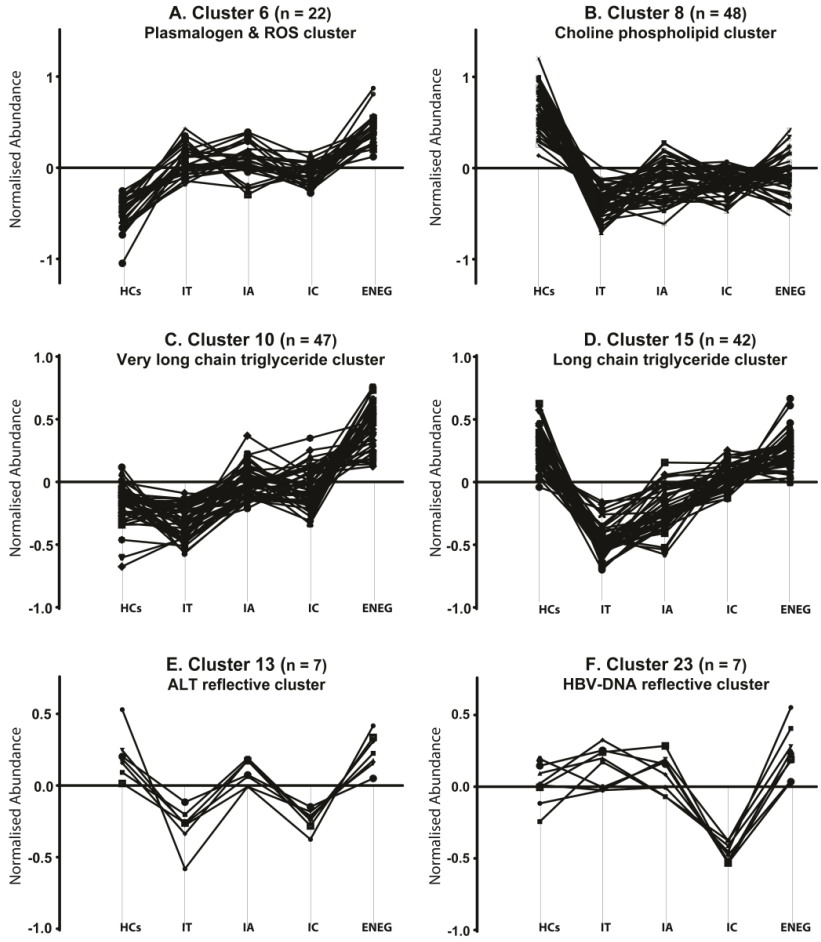

Figure 6.3: Serum Metabolite pattern analyses. a Cluster 6, the plasmalogen & ROS cluster showed a "stable" elevated trend against the HCs during the progression of the four clinical phases. **b** Cluster 8, the choline phospholipid cluster showed a "stable" reduced trend over the four clinical phases against the HCs. **c** Cluster 10, the long chain triglyceride cluster represents metabolites with subtle changes at the start of chronic HBV, but increased significantly over the progression of the four clinical phases. **d** Cluster 15, the short and medium chain triglyceride cluster, grouped metabolites with a significant reduction between the HCs and the

IT phase, after which their levels increased again as the disease progressed. **e** Cluster 13, the ALT reflective cluster, grouped metabolites following the same trend as ALT with increased levels in the IA and ENEG phases. **f** Cluster 23, the HBV DNA cluster represents metabolites reflective of HBV DNA levels, which has its lowest levels during the IC phase. The y-axis is the abundance of metabolites normalized to the overall mean of the metabolite across all samples

Table 6.4: Significant serum metabolites identified changing over the progression of chronic HBV. The significant metabolites are divided into their clusters indicative of their trend and all had an ANOVA *p* value < 0.05.

Targeted Metabolomics Platform	Metabolite class	Metabolite species identified as significant changing during the progression of chronic HBV
Cluster 6 - Stable Increased		
Amines	Amines	Carnitine; Ornithine
Cluster 8 - Stable Decreased		
Acyl-carnitines	Acylcarnitines	Nonaylcarnitine
Negative lipids	Lysophosphatidylcholine (LPC)	*sn1*-C20:3 (w3w6); *SN*2-C20:3 (w3w6)
Cluster 10 - Increasing over the four phases		
Acyl-carnitines	Acylcarnitines	Isovalerylcarnitine; 2-Methylbutyroylcarnitine; Stearoylcarnitine
Amines	Amino acids	Phenylalanine, Glutamic acid, Methionine
	Amines	Choline
Positive lipids	Diacylglycerol (DG)	C36:2
	Triglycerides (TG)	C54:2; C54:3; C54:4; C55:3; C56:3; C56:4; C56:5; C56:6; C58:5
Negative lipids	Free Fatty acids	C20:4 (w6)
Cluster 13 - Reflective of ALT levels		
Amines	Amino acid metabolite	Kynurenine
Cluster 15 - Increasing over the four phases		
Positive lipids	Phosphatidylcholine (PC)	C38:4
	Sphingomeylins (SM)	C18:1/25:0
	Triglycerides (TG)	C42:1; C52:2; C55:2
Negative lipids	Lysophosphatidylethanolamine (LPE)	C18:1; C20:3 (w3w6); C20:4
Cluster 23 - Reflective of HBV-DNA levels		
Acyl-carnitines	Acylcarnitines	Decanoylcarnitine
Negative Lipids	Free Fatty acids	FA C20:3 (w3w6), FA C22:4

Metabolite clusters showing a "stable" increased or decreased trend over the four clinical phases of chronic HBV

Cluster 6 (Fig. 6.3a), and 8 (Fig. 6.3b) represent metabolites significantly altered in the IT phase compared to HCs, and of which the alteration persisted across the progression of chronic HBV with stable increased or decreased trends. Cluster 6 contained 7 plasmalogen phospholipid and lysophospholipid species, of which three were found significantly up-regulated in the IT phase compared to the HCs, having sustained increased levels across the four clinical phases. We named this cluster the "ROS-plasmalogen cluster". Four non-enzymatic route oxylipins, 10-, 11-, 13-, and 14-HDoHEs, grouped within cluster 6 indicate maintained oxidative stress experienced during the progression of chronic HBV. Interestingly, the choline catabolic

metabolites betaine and sarcosine were also within the ROS-plasmalogen cluster, which may suggest some degree of choline metabolism perturbation. The amine metabolites carnitine and ornithine were identified as significantly changing over the clinical phases (Table 6.4). Carnitine is the free fatty acid transporter metabolite and indicates significant dysregulation during chronic HBV ($p<0.001$). The IT and IC phases had lower carnitine levels compared to the IA and ENEG phases reflecting increased energy requirements during these phases. Ornithine is a urea cycle intermediate together with citrulline (cluster 9, $p=0.006$) indicating a dysregulated urea cycle, worsening with the progression of chronic HBV as both had their highest levels in the ENEG phase.

Cluster 8 represents the opposite trend, showing a stable decline of metabolite levels across the four clinical phases compared to HCs. Cluster 8 was labelled the "choline phospholipid cluster", as it comprises 14 phosphatidylcholines and 21 lysophosphatidylcholines. The strong initial reduction of choline phospholipids together with the subsequent maintenance of the reduced levels over the four clinical phases, hints towards an imprinted metabolic alteration. Only the *sn1*- and *sn2*-lysophosphatidylcholine C20:3 species showed significant fluctuations during the progression of the clinical phases (Table 6.4). Three amines, including saccharopine, glutathione and γ-glutamyl glutamine, had stable decreased levels compared to HCs. The glutathione levels reflect diminished antioxidant capacity during chronic HBV, supporting the increased levels of lipid peroxidation products observed within cluster 6.

Metabolite clusters showing an increasing trend over the clinical phases of chronic HBV

From the 24 clusters, number 10 (Fig. 6.3c) and 15 (Fig. 6.3d) were the most densely clustered containing 47 and 42 metabolites, respectively. Both clusters showed an increasing trend across the four clinical phases of chronic HBV, with their defining difference observed when taking the HCs into account.

Cluster 10 shows subtle changes between the HCs and the IT phase, but had a significant increase during the progression of chronic HBV to levels well above HC levels in the ENEG phase. Cluster 10 is dominated by 13 amino acids and 17 triglyceride species, composed of very long acyl species with a combined acyl chain length of between C54 to C60. Thus, this cluster is called the "very long chain triglyceride cluster". During the progression over the four clinical phases, 9 of the 17 triglycerides were identified as significantly increasing, revealing a perturbed triglyceride metabolism (Table 6.4). The essential amino acids methionine and phenylalanine were identified as significantly changing over the clinical phases, and have both been identified as markers of hepatic injury and had their highest levels in the ENEG phase [33–35]. Choline identified as significant and clustered within pattern 10 is an integral part of the glycerophospholipid and sphingolipid metabolism acting as a functional lipid moiety. The increasing choline levels oppose that of its elevated catabolic metabolites betaine and sarcosine (cluster 6).

Cluster 15 shows metabolites that presented with a significant reduction in the IT phase compared to the HC, after which metabolite levels started to increase back to HC levels. More than half of the 42 metabolites in cluster 15, consisted of triglycerides, with a combined acyl chain length ranging from C42 to C55, effectively labelling this the "long chain triglyceride cluster". These results show a biphasic triglyceride response during

chronic HBV. Three of the five clustered lysophosphatidylethanolamines species including C18:1, C20:3 and C20:4 were subsequently identified as significantly increasing over the four clinical phases with levels almost resembling the HCs in the ENEG phase. These results also show that lysophosphatidylethanolamines (cluster 15) responds differently during chronic HBV than lysophosphatidylcholines (cluster 8).

Metabolite clusters correlating to ALT and HBV DNA levels.

During chronic HBV infection, ALT levels (Fig. 6.1a) were highest during the IA and ENEG phases, whereas HBV DNA levels (Fig. 6.1b) were high in the IT, IA and ENEG phases and lowest in the IC phase. Cluster 13 (Fig. 6.3e) and 23 (Fig. 6.3f) represented metabolites correlating to ALT and HBV DNA levels, respectively.

Kynurenine identified in cluster 13 correlated to ALT levels, and had significantly higher levels in the IA and ENEG phases compared to the IT and IC phases (Table 6.4). Kynurenine and its precursor amino acid tryptophan (cluster 15) were both also identified as significantly down-regulated during the IT phase compared to the HCs. Due to these fluctuating levels during the progression of chronic HBV, we inspected the tryptophan/kynurenine ratio relating to indoleamine 2,3-dioxygenase (IDO) activity. The tryptophan/kynurenine ratio had a p-value of 0.038 across the 5 groups with a reduced IDO ratio in the IT, IA, and IC phases of chronic HBV compared to an ENEG phase ratio comparable to the HCs, implying altered IDO regulation during the first three phases of chronic HBV.

Cluster 23, reflecting HBV DNA levels during chronic HBV, consisted solely of five acyl-carnitines and four free fatty acids. The very long chain free fatty acids C20:3 (ω3/ω6) and C22:4 together with decanoylcarnitine had significantly lower levels in the IC phase compared to the other clinical phases possibly correlating to HBV-induced secreted phospholipases [36,37].

Discussion

The present study is the first targeted and biology driven metabolomics profiling of chronic HBV characterising the natural progression through its distinct clinical phases. With the liver being the central organ in nutritional regulation and metabolism, it is not surprising that chronic HBV infections have been shown to induce multiple metabolic alterations in lipid metabolism of the host [15–21]. However, these studies have not addressed and positioned metabolic changes in relation to the progression of chronic HBV disease.

The IT phase is clinically characterised with high levels of HBV replication and minimal hepatic injury. We now show that this phase exhibits major lipid alterations with increased free fatty acids, acyl-carnitines and plasmalogens concurrently with decreased triglyceride, phospholipid (ester-linked), and sphingomyelin levels visualised in Fig. 6.4. The glycolysis intermediate dihydroxyacetone phosphate (DHAP) is the precursor metabolite via glycerol-3-phosphate (G3P) for the *de novo* glycerophospholipids and triglyceride synthesis pathways. Alternatively, DHAP can also be transported to the peroxisomes where it is the precursor for the synthesis of vinyl ether-linked plasmalogen phospholipids. The reaction of DHAP to G3P is catalysed by

glycerol-3-phosphate dehydrogenase (GPDH) and is known as the G3P-NADH shuttle, simultaneously converting NADH to NAD^+ necessary during the glycolysis cycle. Our results suggest that HBV hijacks this G3P-NADH shuttle resulting in reduced levels of glycerophospholipids, lysoglycerophospholipids, triglycerides and sphingomyelins. The secretion of glycerophospholipids from the liver is the main contributor to their serum levels, substantiating the hepatic metabolic fingerprint and the link to HBV activity [38]. Plasmalogen phosphatidylcholine has been identified as the preferred lipid species in the viral envelope and surface antigen particles of HBV, accounting for approximately 60% of total lipid content [39]. Additionally, Li et al., 2015 reported the upregulation of mRNA transcripts in the phosphatidylcholine biosynthesis pathway during HBV infection in HepG2 cell lines, and its necessity for HBV replication [16]. Collectively, the observed increase in choline plasmalogen levels reveals the metabolic engineering capacity of HBV, and supports our HBV hijacking hypothesis of the G3P-NADH shuttle.

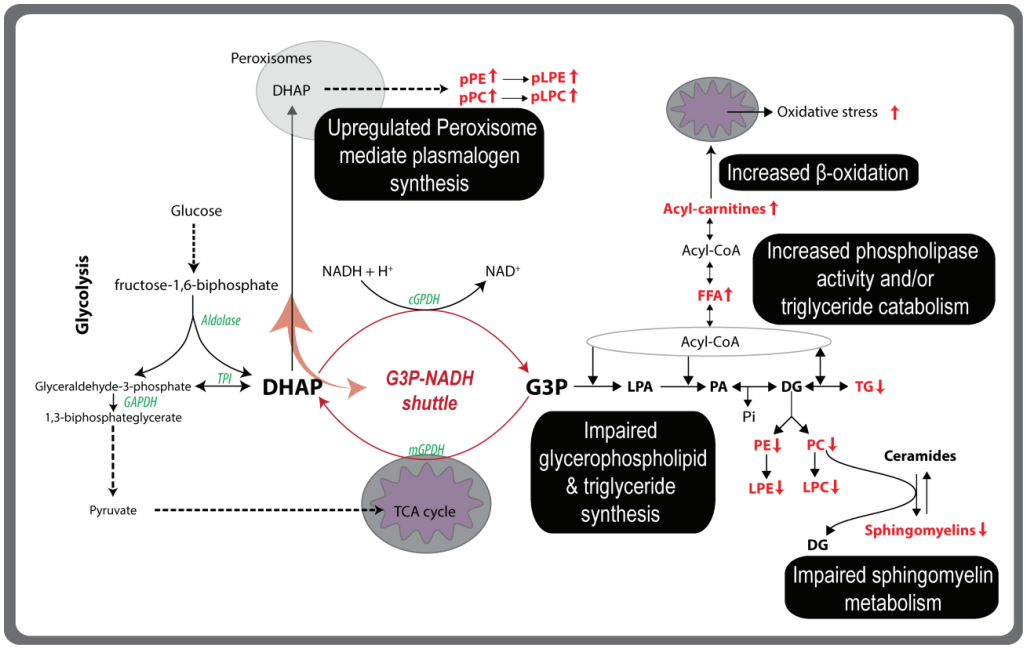

Figure 6.4: Metabolic alterations identified in the IT phase of chronic HBV. Increased levels of DHAP derived plasmalogen phospholipids species, free fatty acids and acyl carnitines were found. A significant decrease in glycerophospholipids, triglycerides and sphingomyelins were found, suggesting the HBV hijacking of the cytosolic glycerol-3-phosphate dehydrogenase (GPDH) enzyme favouring the synthesis of plasmalogen lipid species. Detected metabolic species are highlighted in red with the arrow indicating its trend. DHAP: dihydroxyacetone phosphate, G3P: glycerol-3-phosphate, LPA: lysophosphatidic acid, PA: phosphatidic acid, DG: diacylglycerol, PE: phosphatidylethanolamine, PC: phosphatidylcholine, LPE: lysophosphatidylethanolamine, LPC: lysophosphatidylcholine, TG: triglyceride, FFA: free fatty acids, pPE: plasmalogen phosphatidylethanolamine, pPC: plasmalogen phosphatidylcholine, pLPE: plasmalogen

lysophosphatidylethanolamine, pLPC: plasmalogen lysophosphatidylcholine, GAPDH: glyceraldehyde-3-phosphate dehydrogenase, TPI: triosephosphate isomerase, cGPDH: cytosolic glycerol-3-phosphate dehydrogenase, mGPDH: mitochondrial glycerol-3-phosphate dehydrogenase

Importantly, this altered lipid profile of down-regulated phospholipids and increased plasmalogens persists during the progression of chronic HBV (Fig 6.3*A* & *B*), even during the IC phase where virtually no HBV replication is taking place, implies a HBV induced metabolic imprinting effect. Although other reasons, such as an altered metabolic flux or consumption rate of metabolites and even diet, could be used to explain metabolic observations, the use of pattern analyses and the progressive nature of our clinical phase-defined chronic HBV samples provides concrete evidence to illustrate an altered metabolic state.

During the natural progression of chronic HBV, we measured increased choline, methionine, and very long acyl chain triglyceride levels together with reduced phosphatidylcholine and lysophosphatidylcholine levels, indicating a perturbed choline metabolism. Dietary choline and methionine depravation is strongly interlinked with the development of steatosis, non-alcoholic fatty liver disease, cirrhosis and HCC [40–43]. During conditions of choline restriction, the reduced levels of phosphatidylcholine, a critical component of the VLDL particle, impair hepatic lipoprotein synthesis and results in the accumulation of free triglycerides within hepatocytes [44,45]. Decreased phosphatidylcholine species in the presence of high choline levels during the IA, IC and ENEG phases support the permanent G3P-NADH shuttle hijacking hypothesis, impairing lipoprotein synthesis during chronic HBV, while also explaining the accumulation of triglycerides. Even with decreased levels of long chain free fatty acids in the IC phase, no attenuation of long chain triglycerides levels was observed in this phase. The stable elevated levels of betaine, sarcosine, and methionine indicate enhanced choline catabolism, while increased levels of methionine are also reflective of hepatic injury [34,35]. Previous studies demonstrated that host factors were responsible for the development of steatosis rather than viral factors [46,47]. Our metabolomics data suggest that initiation of steatosis may be a consequence of HBV hijacking of the host's glycerophopholipid metabolism, as liver fat content closely correlates with serum triglyceride levels [48,49].

Another metabolic pathway with increased activity reflective of the natural progression of chronic HBV is composed of urea cycle intermediates: enhanced levels of citrulline and ornithine were detected in the IC and ENEG phases, respectively. The urea cycle is predominantly active in hepatocytes and responsible for detoxifying ammonia. Moreover, the urea cycle has an intimate relationship with the aspartate-malate NADH shuttle functioning across the mitochondrial membrane. One could speculate that the HBV hijacking of the G3P-NADH shuttle, as explained above, will affect the redox status ($NADH/NAD^+$) of the cell and cause an up-regulation/stress of the malate-aspartate $NADH/NAD^+$ shuttle to rectify this imbalance, as shown in Fig. 6.5. The mitochondrial transporter citrin (AGC), encoded for by the gene SLC25A13, is responsible for the transport of aspartate and glutamate during the aspartate-malate NADH shuttle. Cytosolic aspartate binds to citrulline, forming the urea cycle intermediate argininosuccinate, producing arginine and forms ornithine, through releasing urea. We detected increased levels of citrulline, ornithine and glutamate, all implicating impaired aspartate transport, and may reflect reduced integrity and functioning of the mitochondrial citrin

transporter. A dysregulated urea cycle precedes the histological manifestations of irreversible liver damage [50], and thus might be a prediction marker for chronic HBV progression and severity.

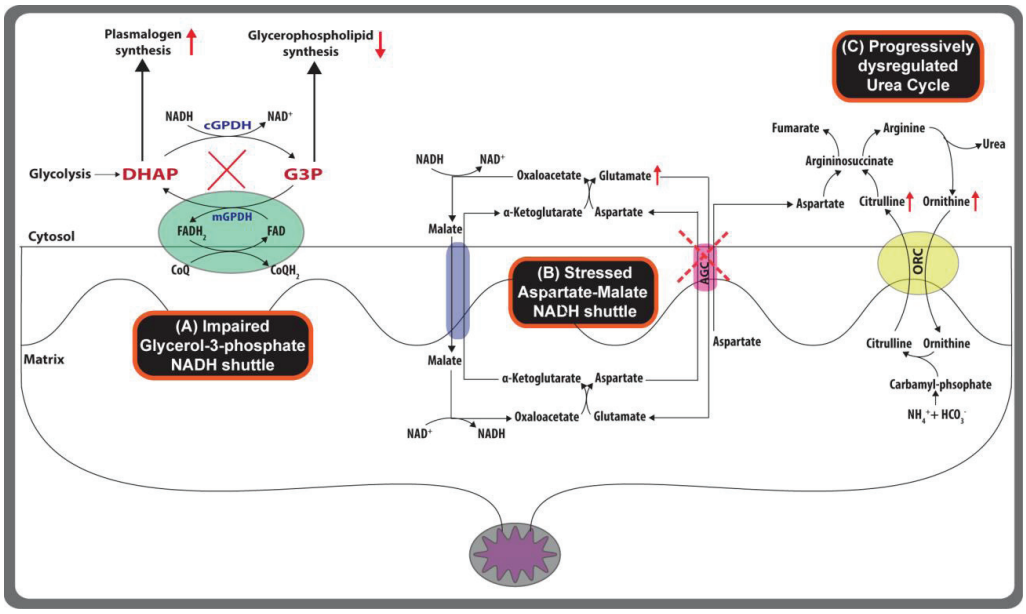

Figure 6.5: Cellular NADH shuttles and the Urea cycle. Schematic representing the interplay between (a) the reduced glycerol-3-phosphate NADH shuttle and (b) a stressed aspartate-malate NADH shuttle and its influence on (c) the urea cycle. The aspartate transporter AGC (aka citrin), facilitates the transport of aspartate across the mitochondrial membrane to the cytosol where it binds to citrulline in the urea cycle to help detoxify ammonium. Ineffective aspartate transport will lead to the accumulation of glutamate, citrulline and ornithine identified in the IC and ENEG clinical phases of HBV infection.

Collectively, the data presented here is the first metabolic study on the natural progression of chronic HBV using patient samples. We found an impaired choline glycerophospholipid metabolism across the four chronic HBV clinical phases, together with increasing concentrations of triglyceride levels and urea cycle intermediates as a liver metabolic fingerprint of the progression of chronic HBV. This metabolic fingerprint relates to the HBV hijacking of the G3P-NADH shuttle, a key player in the plasmalogen, choline and glycerophospholipid metabolic pathways, and its potential as a therapeutic target deserves further investigation. Elegant work done by Zeissig et al., demonstrated the role of lysophospholipids as endogenous antigenic lipid species able to illicit protective immunological responses, which enhanced HBV clearance during acute infection [36]. This may imply that, in addition to redirecting host lipid metabolism to produce the plasmalogens, hijacking of the glycerophospholipid metabolism during acute HBV infection could act as a switch to determine HBV clearance or persistence. Furthermore, the diabetes drug metformin, which inhibits glycerophosphate

dehydrogenase (mGPDH) [51] part of the G3P-NADH shuttle, was found to inhibit HBV protein production and replication [52]. These findings substantiate the therapeutic value of the G3P-NADH shuttle in chronic HBV.

Conclusions

The present study provides many leads and insights to design follow-up studies and at the same time highlights the need of a systems biology approach to better understand chronic HBV. We identified liver related metabolic and injury perturbations, which reflect the natural progression of the disease. The altered glycerophospholipid metabolism in the IT phase attributed to the HBV hijacking of the G3P-NADH shuttle has an intimate relationship with the persisting lipid dysregulation observed in the IA, IC and ENEG clinical phases. Increased levels of the very long chain triglycerides in the IA phase and urea cycle intermediates in the IC phase highlight the risk for developing secondary liver complications during chronic HBV. These metabolites might prove useful as markers of disease progression and severity.

Acknowledgements

This study was supported by the NWO-ZonMW grant number 435002027, and the Virgo consortium, funded by the Dutch government project number FES0908. We would also like to thank the technical staff including L Lamont, B Gonzalez Amoros and H. Elfrink at the Netherlands Metabolomics Centre, Leiden University for performing the metabolomics sample analyses.

References

1. Locarnini, S., Hatzakis, A., Chen, D.-S. & Lok, A. Strategies to control hepatitis B: Public policy, epidemiology, vaccine and drugs. *J. Hepatol.* **62,** S76–86 (2015).
2. Fattovich, G., Bortolotti, F. & Donato, F. Natural history of chronic hepatitis B: special emphasis on disease progression and prognostic factors. *J. Hepatol.* **48,** 335–352 (2008).
3. Kwon, H. & Lok, A. S. Hepatitis B therapy. *Nat. Rev. Gastroenterol. Hepatol.* **8,** 275–284 (2011).
4. Inuzuka, T., Takahashi, K., Chiba, T. & Marusawa, H. Mouse models of hepatitis B virus infection comprising host-virus immunologic interactions. *Pathogens* **3,** 377–389 (2014).
5. Ishida, Y. *et al.* Novel robust in vitro hepatitis B virus infection model using fresh human hepatocytes isolated from humanized mice. *Am. J. Pathol.* **185,** 1275–85 (2015).
6. Putri, S. P. *et al.* Current metabolomics: practical applications. *J. Biosci. Bioeng.* **115,** 579–89 (2013).
7. Shulaev, V. Metabolomics technology and bioinformatics. *Brief. Bioinform.* **7,** 128–39 (2006).
8. Kell, D. B. Metabolomics and systems biology: Making sense of the soup. *Curr. Opin. Microbiol.* **7,** 296–307 (2004).
9. Xiao, J. F., Zhou, B. & Ressom, H. W. Metabolite identification and quantitation in LC-MS/MS-based metabolomics. *Trends Analyt. Chem.* **32,** 1–14 (2012).
10. Ramautar, R., Berger, R., van der Greef, J. & Hankemeier, T. Human metabolomics: strategies to understand biology. *Curr. Opin. Chem. Biol.* **17,** 841–846 (2013).
11. Pacchiarotta, T., Deelder, A. M. & Mayboroda, O. A. Metabolomic investigations of human infections. *Bioanalysis* **4,** 919–25 (2012).

12. Vinayavekhin, N., Homan, E. A. & Saghatelian, A. Exploring disease through metabolomics. *ACS Chem. Biol.* **5,** 91–103 (2010).
13. Munger, J., Bajad, S. U., Coller, H. A., Shenk, T. & Rabinowitz, J. D. Dynamics of the cellular metabolome during human cytomegalovirus infection. *PLoS Pathog.* **2,** e132 (2006).
14. Vastag, L., Koyuncu, E., Grady, S. L., Shenk, T. E. & Rabinowitz, J. D. Divergent effects of human cytomegalovirus and herpes simplex virus-1 on cellular metabolism. *PLoS Pathog.* **7,** e1002124 (2011).
15. Chen, S. *et al.* Serum lipid profiling of patients with chronic hepatitis B, cirrhosis, and hepatocellular carcinoma by ultra fast LC/IT-TOF MS. *Electrophoresis* **34,** 2848–2856 (2013).
16. Li, H. *et al.* The metabolic responses to hepatitis B virus infection shed new light on pathogenesis and targets for treatment. *Sci. Rep.* **5,** 8421 (2015).
17. Teng, C.-F. *et al.* A biphasic response pattern of lipid metabolomics in the stage progression of hepatitis B virus X tumorigenesis. *Mol. Carcinog.* **55,** 105–14 (2016).
18. Kwarteng, J., Owusu, L. & Afihene, M. Lowered serum triglyceride levels among chronic hepatitis B-infected patients in Ghana. *J. Sci. Technol.* **32,** 1–10 (2012).
19. Zheng, S.-J. *et al.* Serum sphingomyelin has potential to reflect hepatic injury in chronic hepatitis B virus infection. *Int. J. Infect. Dis.* **33,** 149–155 (2015).
20. Zhou, L. *et al.* Serum metabolomics reveals the deregulation of fatty acids metabolism in hepatocellular carcinoma and chronic liver diseases. *Anal. Bioanal. Chem.* **403,** 203–213 (2012).
21. Zhang, A., Sun, H., Han, Y., Yan, G. & Wang, X. Urinary metabolic biomarker and pathway study of hepatitis B virus infected patients based on UPLC-MS system. *PLoS One* **8,** 1–8 (2013).
22. Sun, S. *et al.* Differences of Excess and Deficiency Zheng in Patients with Chronic Hepatitis B by Urinary Metabonomics. *Evidence-Based Complement. Altern. Med.* **2013,** 1–10 (2013).
23. Soga, T. *et al.* Serum metabolomics reveals γ-glutamyl dipeptides as biomarkers for discrimination among different forms of liver disease. *J. Hepatol.* **55,** 896–905 (2011).
24. Xue, R. *et al.* Gas chromatography/mass spectrometry screening of serum metabolomic biomarkers in hepatitis B virus infected cirrhosis patients. *Clin. Chem. Lab. Med.* **47,** 305–310 (2009).
25. Beyoğlu, D. *et al.* Tissue metabolomics of hepatocellular carcinoma: Tumor energy metabolism and the role of transcriptomic classification. *Hepatology* **58,** 229–238 (2013).
26. Yin, P. *et al.* A metabonomic study of hepatitis B-induced liver cirrhosis and hepatocellular carcinoma by using RP-LC and HILIC coupled with mass spectrometry. *Mol. Biosyst.* **5,** 868–876 (2009).
27. Association, E. EASL Clinical Practice Guidelines: Management of chronic hepatitis B virus infection. *J. Hepatol.* **57,** 167–185 (2012).
28. Noga, M. J. *et al.* Metabolomics of cerebrospinal fluid reveals changes in the central nervous system metabolism in a rat model of multiple sclerosis. *Metabolomics* **8,** 253–263 (2012).
29. Hu, C. *et al.* RPLC-ion-trap-FTMS method for lipid profiling of plasma: method validation and application to p53 mutant mouse model. *J. Proteome Res.* **7,** 4982–91 (2008).
30. Strassburg, K. *et al.* Quantitative profiling of oxylipins through comprehensive LC-MS/MS analysis: application in cardiac surgery. *Anal. Bioanal. Chem.* **404,** 1413–26 (2012).
31. Xia, J., Sinelnikov, I. V., Han, B. & Wishart, D. S. MetaboAnalyst 3.0—making metabolomics more meaningful. *Nucleic Acids Res.* **43,** W251–W257 (2015).
32. Xia, J. & Wishart, D. S. Web-based inference of biological patterns, functions and pathways from metabolomic data using MetaboAnalyst. *Nat. Protoc.* **6,** 743–760 (2011).
33. Dicpinigaitis, P. V, Bhat, R., Rhoton, W. a, Tibb, A. S. & Negassa, A. Effect of viral upper respiratory

tract infection on the urge-to-cough sensation. *Respir. Med.* **105,** 615–8 (2011).
34. Morgan, M. Y., Marshall, A. W., Milsom, J. P. & Sherlock, S. Plasma amino-acid patterns in liver disease. *Gut* **23,** 362–70 (1982).
35. Lieber, C. S. S-Adenosyl-L-methionine: Its role in the treatment of liver disorders. *Am. J. Clin. Nutr.* **76(suppl),** 1183–1187S (2002).
36. Zeissig, S. *et al.* Hepatitis B virus–induced lipid alterations contribute to natural killer T cell–dependent protective immunity. *Nat. Med.* **18,** 1060–1068 (2012).
37. Ito, M. *et al.* Distribution of type V secretory phospholipase A2 expression in human hepatocytes damaged by liver disease. *J. Gastroenterol. Hepatol.* **19,** 1140–9 (2004).
38. Quehenberger, O. & Dennis, E. A. The human plasma lipidome. *N. Engl. J. Med.* **365,** 1812–23 (2011).
39. Satoh, O., Umeda, M., Imai, H., Tunoo, H. & Inoue, K. Lipid composition of hepatitis B virus surface antigen particles and the particle-producing human hepatoma cell lines. *J. Lipid Res.* **31,** 1293–1300 (1990).
40. Corbin, K. D. & Zeisel, S. H. Choline metabolism provides novel insights into nonalcoholic fatty liver disease and its progression. *Current Opinion in Gastroenterology* **28,** 159–165 (2012).
41. Zeisel, S. H. & Blusztajn, J. K. Choline and human nutrition. *Annu. Rev. Nutr.* **14,** 269–296 (1994).
42. Ghoshal, A. K. & Farber, E. The induction of liver cancer by dietary deficiency of choline and methionine without added carcinogens. *Carcinogenesis* **5,** 1367–1370 (1984).
43. Ghoshal, A. K., Ahluwalia, M. & Farber, E. The rapid induction of liver cell death in rats fed a choline-deficient methionine-low diet. *Am. J. Pathol.* **113,** 309–314 (1983).
44. Gibbons, G. F. Assembly and secretion of hepatic very-low-density lipoprotein. *Biochem J.* **286,** 1–13 (1990).
45. Mason, T. M. The role of factors that regulate the synthesis and secretion of very-low-density lipoprotein by hepatocytes. *Crit. Rev. Clin. Lab. Sci.* **35,** 461–487 (1998).
46. Peng, D., Han, Y., Ding, H. & Wei, L. Hepatic steatosis in chronic hepatitis B patients is associated with metabolic factors more than viral factors. *J. Gastroenterol. Hepatol.* **23,** 1082–1088 (2008).
47. Machado, M. V, Oliveira, A. G. & Cortez-Pinto, H. Hepatic steatosis in hepatitis B virus infected patients: meta-analysis of risk factors and comparison with hepatitis C infected patients. *J. Gastroenterol. Hepatol.* **26,** 1361–7 (2011).
48. Adiels, M. *et al.* Overproduction of large VLDL particles is driven by increased liver fat content in man. *Diabetologia* **49,** 755–765 (2006).
49. Marchesini, G. *et al.* Nonalcoholic fatty liver disease: a feature of the metabolic syndrome. *Diabetes* **50,** 1844–1850 (2001).
50. Maier, K. P., Talke, H. & Gerok, W. Activities of urea-cycle enzymes in chronic liver disease. *Klin. Wochenschr.* **57,** 661–5 (1979).
51. Madiraju, A. K. *et al.* Metformin suppresses gluconeogenesis by inhibiting mitochondrial glycerophosphate dehydrogenase. *Nature* **510,** 542–6 (2014).
52. Xun, Y.-H. *et al.* Metformin inhibits hepatitis B virus protein production and replication in human hepatoma cells. *J. Viral Hepat.* **21,** 597–603 (2014).

Chapter 6 Supplementary information

Supplementary Figures

PCA scores plot

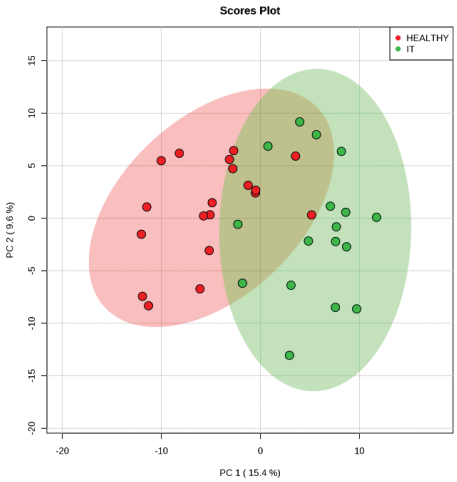

Figure S6.1: HCs vs IT phase PCA analyses. PCA analyses plotting PC1 vs. PC2 for the HCs (Red) versus the IT phase (Green), using the fused data set comprising of 37 cases and all 314 detected metabolites. Natural group clustering lead to partial differentiation between the two groups, indicating metabolic differences between them.

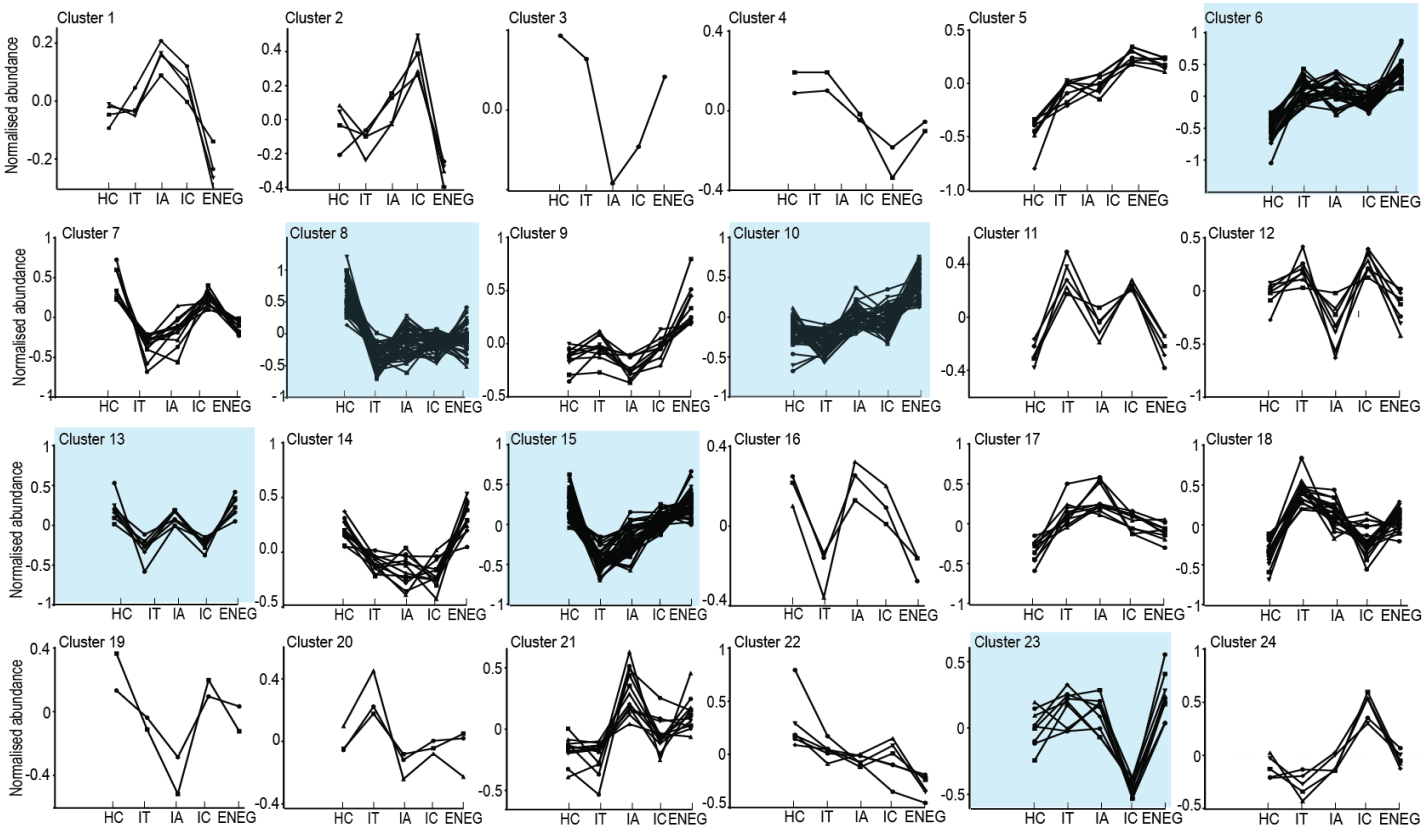

Figure. S6.2: K-means clustering. Metabolites are grouped into different classes by K-means clustering based on the changes of their abundance during the progression of chronic HBV. Expression pattern-based analysis was performed with all 314 metabolites and 88 patients. A K-means clustering was performed in MATLAB using *kmeans* on these metabolites in order to examine alterations in their measurement during the course of chronic HBV. Within each cluster metabolites present similar expression patterns, while different from metabolites in other clusters. The 24 clusters present the best partition of all 314 metabolites and are shown in the figure, with the blue highlighted clusters being discussed in the main text. The x-axis shows the healthy controls (HC) and the four clinical phases (IT, IA, IC, and ENEG). The y-axis is the abundance of metabolites normalized to the overall mean of the metabolite across all samples.

Supplementary Tables.

TABLE S6.1. : Descriptive statistics of significant serum metabolites between HCs and the IT phase. The table contains their corresponding statistical scores and descriptive statistics using normalised area ratios, ordered by metabolic class.

Targeted Metabolomics Platform	Metabolite	T-Test	False discovery rate	Fold change	Healthy Controls	IT Phase
		p-value	*q*-value	(FC)	Mean ± SD	Mean ± SD
			Phospholipids			
Positive Lipids	PC C32:1	0.0012	0.006	0.51	0.68 ± 0.44	0.35 ± 0.22
	PC C32:2	< 0.0001	< 0.001	0.52	0.19 ± 0.06	0.1 ± 0.04
	PC C34:1	0.0029	0.010	0.76	7.74 ± 1.9	5.91 ± 1.52
	PC C34:3	0.0001	0.001	0.64	0.67 ± 0.22	0.43 ± 0.14
	PC C34:4	< 0.0001	< 0.001	0.45	0.06 ± 0.02	0.03 ± 0.01
	PC C36:3	< 0.0001	0.001	0.72	6.36 ± 1.65	4.62 ± 0.86
	PC C36:4	0.0006	0.003	0.75	7.2 ± 1.64	5.47 ± 1.1
	PC C36:6	0.0134	0.035	0.72	0.03 ± 0.01	0.02 ± 0.01
	PC C38:3	0.0063	0.018	0.7	1.37 ± 0.49	0.96 ± 0.37
	PE C38:4	< 0.0001	< 0.001	0.6	0.33 ± 0.1	0.2 ± 0.07
			Plasmalogens			
Positive Lipids	pPC C34:2	0.0003	0.002	1.37	0.29 ± 0.08	0.4 ± 0.1
	pPC C36:2	0.0005	0.003	1.25	0.09 ± 0.02	0.12 ± 0.02
	pPC C36:3	0.0005	0.003	1.3	0.07 ± 0.02	0.1 ± 0.02
	pPC C38:6	0.0025	0.009	1.6	0.16 ± 0.03	0.22 ± 0.08
	pPE C38:5	0.002	0.008	1.42	0.19 ± 0.06	0.28 ± 0.09
	pPE C38:7*	0.0229	0.052	1.4	0.07 ± 0.02	0.1 ± 0.03
			Lysophospholipids			
Negative Lipids	LPE C18:0	0.0002	0.002	0.65	0.13 ± 0.03	0.08 ± 0.03
	LPE C18:1	0.0027	0.008	0.66	0.07 ± 0.03	0.05 ± 0.02
	LPE C18:2*	0.025	0.052	0.71	0.14 ± 0.07	0.10 ± 0.05
	LPE C20:3 (w3w6)	0.0002	0.001	0.54	0.008 ± 0.003	0.005 ± 0.002
	LPE C20:4	0.0008	0.003	0.72	0.079 ± 0.023	0.058 ± 0.015
	LPE C22:5 (w3)*	0.0249	0.052	0.75	0.008 ± 0.003	0.006 ± 0.002
	sn1 LPC C14:0	< 0.0001	< 0.001	0.47	0.19 ± 0.06	0.09 ± 0.03
	sn1 LPC C15:0	< 0.0001	< 0.001	0.63	0.1 ± 0.02	0.06 ± 0.02
	sn1 LPC C16:1	0.0002	0.001	0.71	0.35 ± 0.09	0.25 ± 0.07
	sn1 LPC C18:1	< 0.0001	< 0.001	0.73	4.04 ± 0.67	2.99 ± 0.68
	sn1 LPC C18:2	0.0081	0.02	0.79	8.0 ± 2.1	6.4 ± 1.6
	sn1 LPC C18:3 (w3w6)	< 0.0001	< 0.001	0.55	0.118 ± 0.041	0.065 ± 0.031
	sn1 LPC C20:3 (w3w6)	< 0.0001	< 0.001	0.53	0.82 ± 0.33	0.44 ± 0.15
	sn1 LPC C20:3 (w9)	< 0.0001	< 0.001	0.46	0.034 ± 0.017	0.015 ± 0.008
	sn1 LPC C20:4	0.0003	0.001	0.69	1.84 ± 0.52	1.28 ± 0.35
	sn1 LPC C22:4	0.008	0.02	0.67	0.053 ± 0.02	0.035 ± 0.01
	sn1 LPC C22:5 (w6)	0.0015	0.004	0.59	0.042 ± 0.019	0.025 ± 0.01
	sn2 LPC C14:0	< 0.0001	< 0.001	0.46	0.04 ± 0.013	0.018 ± 0.007
	sn2 LPC C16:1	0.0001	< 0.001	0.69	0.068 ± 0.018	0.047 ± 0.013
	sn2 LPC C18:1	< 0.0001	< 0.001	0.74	0.7 ± 0.11	0.52 ± 0.12
	sn2 LPC C18:2	0.0058	0.015	0.77	1.59 ± 0.42	1.24 ± 0.32
	sn2 LPC C18:3 (w3w6)	< 0.0001	< 0.001	0.54	0.02 ± 0.01	0.01 ± 0.01
	sn2 LPC C20:3 (w3w6)	< 0.0001	< 0.001	0.54	0.16 ± 0.06	0.09 ± 0.03
	sn2 LPC C20:4	0.0049	0.013	0.73	0.35 ± 0.11	0.26 ± 0.07
			Lyso-Plasmalogens			
Negative Lipids	pLPC C16:0	0.0006	0.002	1.32	0.1 ± 0.03	0.13 ± 0.02
	pLPC C16:1	0.0035	0.011	1.21	0.03 ± 0.005	0.04 ± 0.006
	pLPC C18:1	0.0001	0.003	1.44	0.068 ± 0.018	0.088 ± 0.017
	pLPC C18:2	0.0017	0.005	1.32	0.014 ± 0.004	0.019 ± 0.004
			Triglycerides			

	TG C42:1	0.0055	0.017	0.42	0.07 ± 0.05	0.03 ± 0.02
	TG C44:2	0.0016	0.007	0.49	0.11 ± 0.07	0.05 ± 0.02
	TG C46:1	< 0.0001	0.001	0.44	0.73 ± 0.43	0.32 ± 0.11
	TG C46:2	< 0.0001	0.001	0.4	0.37 ± 0.22	0.15 ± 0.06
	TG C46:3	0.0015	0.007	0.3	0.09 ± 0.06	0.03 ± 0.02
	TG C48:1	0.0002	0.002	0.4	1.93 ± 1.29	0.79 ± 0.57
	TG C48:2	< 0.0001	0.001	0.4	1.44 ± 0.87	0.58 ± 0.33
	TG C48:3	0.0005	0.003	0.43	0.49 ± 0.3	0.21 ± 0.09
	TG C48:4*	0.0233	0.052	0.52	0.1 ± 0.07	0.05 ± 0.03
	TG C50:0	0.0209	0.049	0.66	0.70 ± 0.43	0.46 ± 0.42
	TG C50:1	0.0017	0.007	0.51	4.05 ± 2.47	2.09 ± 1.67
	TG C50:2	0.0009	0.005	0.55	4.62 ± 2.27	2.55 ± 1.56
Positive Lipids	TG C50:3	0.0019	0.008	0.58	2.23 ± 1.06	1.31 ± 0.62
	TG C50:4	0.009	0.024	0.59	0.65 ± 0.34	0.39 ± 0.18
	TG C50:5	0.0184	0.044	0.57	0.14 ± 0.08	0.08 ± 0.04
	TG C51:1	0.0005	0.003	0.6	0.34 ± 0.15	0.2 ± 0.07
	TG C51:2	0.0005	0.003	0.61	0.48 ± 0.19	0.29 ± 0.11
	TG C51:3	0.0034	0.011	0.66	0.28 ± 0.12	0.19 ± 0.07
	TG C52:1	0.0021	0.008	0.56	1.67 ± 0.98	0.94 ± 0.89
	TG C52:2	0.0028	0.01	0.68	9.1 ± 2.9	6.2 ± 2.6
	TG C54:1	0.0051	0.016	0.65	0.19 ± 0.09	0.12 ± 0.05
	TG C54:2	0.0034	0.011	0.67	1.31 ± 0.44	0.88 ± 0.37
	TG C55:2	0.0001	0.001	0.68	0.08 ± 0.02	0.05 ± 0.02
	TG C56:5	0.0113	0.03	0.75	0.47 ± 0.15	0.36 ± 0.16
	TG C58:5	0.0177	0.043	0.79	0.04 ± 0.01	0.03 ± 0.01
			Amines			
	Kynurenine	0.0008	0.007	0.69	0.008 ± 0.002	0.005 ± 0.001
	Saccharopine	< 0.0001	< 0.001	0.55	0.006 ± 0.002	0.003 ± 0.001
	4-Hydroxyproline	0.0039	0.025	1.68	0.13 ± 0.05	0.23 ± 0.12
	Glutathione	0.0009	0.007	0.72	0.003 ± 0.001	0.002 ± 0.001
Amines	Pipecolic_acid	0.0007	0.007	1.46	1.01 ± 0.23	1.48 ± 0.54
	s_Methylcysteine	0.0074	0.04	1.70	0.2 ± 0.08	0.34 ± 0.19
	Sarcosine*	0.0306	0.129	1.30	0.011 ± 0.004	0.014 ± 0.005
	Tryptophan*	0.013	0.061	0.77	3.65 ± 0.91	2.83 ± 0.59
	γ-Glutamylglutamine	0.0004	0.007	0.65	0.012 ± 0.004	0.007 ± 0.003
Acyl Carnitines	Betaine*	0.0288	0.235	1.33	2.35 ± 0.98	3.13 ± 0.95
			Cholesterol esters			
	CE C18:3	0.017	0.043	0.77	0.04 ± 0.01	0.03 ± 0.01
			Sphingomyelins			
	SM C18:1/14:0	< 0.0001	< 0.001	0.70	0.45 ± 0.1	0.32 ± 0.07
	SM C18:1/21:0	< 0.0001	< 0.001	0.70	0.27 ± 0.05	0.19 ± 0.03
Positive Lipids	SM C18:1/23:0	0.0001	0.001	0.78	0.67 ± 0.12	0.53 ± 0.08
	SM C18:1/25:0	0.0142	0.036	0.64	0.06 ± 0.02	0.04 ± 0.02
	SM C18:1/25:1	0.001	0.005	0.64	0.1 ± 0.03	0.07 ± 0.03
			Free fatty acid and Acyl-carnitines			
	Nonanoylcarnitine	< 0.0001	< 0.001	0.29	0.34 ± 0.14	0.1 ± 0.05
Acyl Carnitines	Oleylcarnitine*	0.0361	0.235	1.38	1.35 ± 0.44	1.87 ± 0.74
	Linoleylcarnitine	0.001	0.013	1.79	0.65 ± 0.28	1.16 ± 0.57
Negative Lipids	FA C20:2	0.0103	0.023	2.21	0.24 ± 0.13	0.53 ± 0.38
	FA C18:2	0.0102	0.023	2.19	13.07 ± 8.16	28.57 ± 21.57
			Oxylipins			
	5-HETrE	0.0001	0.003	0.39	0.03 ± 0.02	0.01 ± 0.01
	11-HDoHE*	0.0037	0.065	2.68	0.02 ± 0.01	0.05 ± 0.04
Oxylipins	14-HDoHE*	0.0194	0.227	2.38	0.29 ± 0.31	0.68 ± 0.72
	8,9-DiHETrE*	0.0347	0.262	0.70	0.01 ± 0.003	0.004 ± 0.002
	10-HDoHE*	0.0442	0.262	1.76	0.04 ± 0.03	0.06 ± 0.05
	12,13-DiHOME*	0.045	0.262	0.53	3.65 ± 2.93	1.94 ± 1.50

* q-value > 0.05

Table S6.2: Pattern analyses K-means serum metabolite scores and assigned clusters (Excel format – Available on request)

Table S6.3: Descriptive statistics of significant serum metabolites between clinical phases. The table contains their corresponding anova p value, pattern analyses cluster and phase descriptive statistics using normalised area ratios, ordered by metabolic class.

Targeted Metabolomics Platform	Metabolite	p-value	Pattern analyse cluster	Healthy Controls Mean ± SD	IT Phase Mean ± SD	IA Phase Mean ± SD	IC Phase Mean ± SD	ENEG Phase Mean ± SD
				Phospholipids				
Positive Lipids	PC C38:4	0.0432	15	3.94 ± 0.94	3.3 ± 0.59	3.15 ± 0.75	3.78 ± 0.95	3.95 ± 0.99
	PC C40:4	0.0478	14	0.08 ± 0.03	0.07 ± 0.03	0.06 ± 0.03	0.06 ± 0.03	0.09 ± 0.04
				Lysophospholipids				
Negative Lipids	*sn1* LPC C20:3 (w3w6)	0.0284	8	0.82 ± 0.33	0.44 ± 0.15	0.49 ± 0.16	0.47 ± 0.16	0.65 ± 0.25
	sn2 LPC C20:3 (w3w6)	0.0263	8	0.16 ± 0.06	0.09 ± 0.03	0.1 ± 0.03	0.09 ± 0.03	0.13 ± 0.05
	LPE C18:1	0.0490	15	0.07 ± 0.03	0.05 ± 0.02	0.06 ± 0.03	0.07 ± 0.03	0.07 ± 0.05
	LPE C20:3 (w3w6)	0.0292	15	0.008 ± 0.003	0.005 ± 0.002	0.006 ± 0.003	0.007 ± 0.003	0.007 ± 0.003
	LPE C20:4	0.0226	15	0.079 ± 0.023	0.058 ± 0.015	0.057 ± 0.019	0.074 ± 0.021	0.073 ± 0.03
	sn1 LPC C20:1	0.0323	21	0.047 ± 0.009	0.045 ± 0.008	0.061 ± 0.016	0.056 ± 0.017	0.054 ± 0.015
				Triglycerides				
Positive Lipids	TG C54:2	0.0268	10	1.31 ± 0.44	0.88 ± 0.37	1.29 ± 0.78	1.23 ± 0.68	2.13 ± 2.14
	TG C54:3	0.0158	10	3.18 ± 0.83	2.64 ± 1.18	3.68 ± 1.84	3.28 ± 1.63	5.26 ± 3.8
	TG C54:4	0.0398	10	3.28 ± 1.33	3.35 ± 1.57	4.69 ± 2.09	3.59 ± 1.66	5.27 ± 3.41
	TG C55:3	0.0249	10	0.09 ± 0.02	0.08 ± 0.02	0.09 ± 0.03	0.09 ± 0.02	0.11 ± 0.03
	TG C56:3	0.0282	10	0.14 ± 0.04	0.12 ± 0.06	0.14 ± 0.07	0.14 ± 0.08	0.26 ± 0.29
	TG C56:4	0.0013	10	0.23 ± 0.06	0.19 ± 0.08	0.25 ± 0.09	0.22 ± 0.11	0.36 ± 0.25
	TG C56:5	0.0025	10	0.47 ± 0.15	0.36 ± 0.16	0.45 ± 0.23	0.41 ± 0.23	0.61 ± 0.26
	TG C56:6	0.0415	10	0.72 ± 0.28	0.6 ± 0.31	0.71 ± 0.34	0.65 ± 0.27	0.86 ± 0.34
	TG C58:5	0.0098	10	0.04 ± 0.01	0.03 ± 0.01	0.04 ± 0.01	0.04 ± 0.01	0.05 ± 0.03
	TG C42:1	0.0428	15	0.07 ± 0.05	0.03 ± 0.02	0.03 ± 0.01	0.06 ± 0.06	0.07 ± 0.09
	TG C52:2	0.0286	15	9.1 ± 2.87	6.24 ± 2.65	7.12 ± 2.89	7.55 ± 3.14	10.79 ± 5.36
	TG C55:2	0.0157	15	0.08 ± 0.02	0.05 ± 0.02	0.06 ± 0.03	0.06 ± 0.02	0.08 ± 0.03
				Amines				
Amines	Ornithine	0.0065	6	1.15 ± 0.27	1.37 ± 0.43	1.41 ± 0.29	1.47 ± 0.45	1.84 ± 0.45
	Phenylalanine	0.0126	10	0.84 ± 0.16	0.83 ± 0.14	0.98 ± 0.1	0.97 ± 0.16	1 ± 0.2
	Glutamic acid	0.0135	10	1.07 ± 0.38	1.14 ± 0.31	1.43 ± 0.42	1.37 ± 0.49	1.73 ± 0.66
	Methionine	0.0392	10	0.015 ± 0.008	0.014 ± 0.014	0.013 ± 0.005	0.015 ± 0.005	0.015 ± 0.006
	Kynurenine	0.0059	13	0.008 ± 0.002	0.005 ± 0.001	0.006 ± 0.002	0.006 ± 0.001	0.007 ± 0.002
	Citrulline	0.0061	9	0.32 ± 0.06	0.31 ± 0.07	0.3 ± 0.08	0.33 ± 0.09	0.4 ± 0.08
Acyl Carnitines	Carnitine	0.0008	6	2.95 ± 0.87	3.26 ± 0.69	3.53 ± 0.73	3.19 ± 0.64	4.01 ± 0.64
	Choline	0.0113	10	1.22 ± 0.26	1.37 ± 0.36	1.89 ± 0.54	1.56 ± 0.4	1.78 ± 0.43

Sphingomyelins								
Positive Lipids	SM C18:1/18:1	0.0112	12	0.35 ± 0.07	0.4 ± 0.05	0.33 ± 0.05	0.4 ± 0.06	0.37 ± 0.07
	SM C18:1/25:0	0.0346	15	0.06 ± 0.02	0.04 ± 0.02	0.04 ± 0.02	0.05 ± 0.02	0.05 ± 0.03
	SM C18:1/23:1	0.0023	7	0.52 ± 0.1	0.43 ± 0.05	0.4 ± 0.06	0.51 ± 0.08	0.45 ± 0.12
	SM C18:1/21:0	0.0231	7	0.27 ± 0.05	0.19 ± 0.03	0.2 ± 0.04	0.24 ± 0.05	0.23 ± 0.08
Free fatty acid and Acyl-carnitines								
Acyl Carnitines	Nonaylcarnitine	0.0168	8	0.34 ± 0.14	0.1 ± 0.05	0.19 ± 0.12	0.16 ± 0.14	0.24 ± 0.18
	Isovalerylcarnitine	0.0097	10	0.83 ± 0.49	0.68 ± 0.29	0.94 ± 0.41	0.78 ± 0.22	1.07 ± 0.47
	Stearoylcarnitine	0.0295	10	0.47 ± 0.15	0.43 ± 0.13	0.5 ± 0.17	0.46 ± 0.13	0.58 ± 0.18
	2-Methylbutyroylcarnitine	0.0390	10	0.59 ± 0.21	0.49 ± 0.18	0.55 ± 0.18	0.53 ± 0.22	0.71 ± 0.29
	Decenoylcarnitine	0.0226	18	1.25 ± 0.64	1.75 ± 1.19	1.74 ± 0.83	1.03 ± 0.58	1.41 ± 0.38
	Decanoylcarnitine	0.0468	23	0.95 ± 0.81	1.02 ± 0.9	0.93 ± 0.5	0.6 ± 0.4	0.89 ± 0.42
Negative Lipids	FA C20:4 (w6)	0.0143	10	6.36 ± 4.91	6.31 ± 2.78	7.08 ± 2.82	5.93 ± 2.94	8.63 ± 3.09
	FA C20:3 (w3w6)	0.0293	23	0.85 ± 0.31	0.9 ± 0.39	0.86 ± 0.33	0.75 ± 0.34	1.09 ± 0.36
	FA C22:4	0.0365	23	0.4 ± 0.16	0.49 ± 0.29	0.41 ± 0.19	0.38 ± 0.23	0.53 ± 0.17
Oxylipins								
Oxylipins	12-HETE	0.0472	14	8.63 ± 15.99	5.71 ± 7.43	6.4 ± 5.77	4.59 ± 2.96	11.19 ± 8.67
	5,6-DiHETrE	0.0486	21	0.017 ± 0.009	0.019 ± 0.014	0.037 ± 0.034	0.019 ± 0.014	0.033 ± 0.025
Diacylglycerol								
Positive Lipids	DG C36:2	0.0354	10	0.26 ± 0.07	0.22 ± 0.08	0.25 ± 0.09	0.24 ± 0.08	0.35 ± 0.17